LAWRENCE
LIVERMORE
NATIONAL
LABORATORY

UCRL-JRNL-225917

Light element isotopic compositions of cometary matter returned by the STARDUST mission

K. D. McKeegan, J. Aleon, J. Bradley, D. Brownlee, H. Busemann, A. Butterworth, M. Chaussidon, S. Fallon, C. Floss, J. Gilmour, M. Gounelle, G. Graham, Y. Guan, P. R. Heck, P. Hoppe, I. D. Hutcheon, J. Huth, H. Ishii, M. Ito, S. B. Jacobsen, A. Kearsley, L. A. Leshin, M.-C. Liu, I. Lyon, K. Marhas, B. Marty, G. Matrajt, A. Meibom, S. Messenger, S. Mostefaoui, K. Nakamura-Messenger, L. Nittler, R. Palma, R. O. Pepin, D. A. Papanastassiou, F. Robert, D. Schlutter, C. J. Snead, F. J. Stadermann, R. Stroud, P. Tsou, A. Westphal, E. D. Young, K. Ziegler, L. Zimmermann, E. Zinner

October 10, 2006

Science

Light element isotopic compositions of cometary matter returned by the STARDUST mission

Kevin D. McKeegan[1*], Jerome Aléon[2,8], John Bradley[3], Donald Brownlee[4], Henner Busemann[5], Anna Butterworth[6], Marc Chaussidon[7], Stewart Fallon[8], Christine Floss[9], Jamie Gilmour[10], Matthieu Gounelle[11], Giles Graham[3], Yunbin Guan[12], Philipp R. Heck[13], Peter Hoppe[13], Ian D. Hutcheon[8], Joachim Huth[13], Hope Ishii[3], Motoo Ito[14], Stein B. Jacobsen[15], Anton Kearsley[16], Laurie A. Leshin[17], Ming-Chang Liu[1], Ian Lyon[10], Kuljeet Marhas[9], Bernard Marty[7], Graciela Matrajt[4], Anders Meibom[11], Scott Messenger[14], Smail Mostefaoui[11], Keiko Nakamura-Messenger[14,18], Larry Nittler[5], Russ Palma[19,20], Robert O. Pepin[20], Dimitri A. Papanastassiou[21], Francois Robert[11], Dennis Schlutter[20], Christopher J. Snead[6], Frank J. Stadermann[9], Rhonda Stroud[22], Peter Tsou[21], Andrew Westphal[6], Edward D. Young[1], Karen Ziegler[1], Laurent Zimmermann[7], Ernst Zinner[9]

Affiliations:
[1] Dept. of Earth and Space Sciences, University of California Los Angeles, Los Angeles, CA. 90095-1567, USA.

[2] Centre de Spectrometrie Nucleaire et de Spectrometrie de Masse, Bat 104, 91405 Orsay Campus, France.

[3] Institute of Geophysics and Planetary Physics, Lawrence Livermore National Laboratory, Livermore, CA. 94550, USA.

[4] Department of Astronomy, University of Washington, Seattle, WA. 98195, USA.

[5] Department of Terrestrial Magnetism, Carnegie Institution of Washington, 5241 Broad Branch Road, NW, Washington, DC. 20015, USA.

[6] Space Sciences Laboratory, University of California, 7 Gauss Way, Berkeley, CA 94720-7450, USA.

[7] Centre de Recherches Petrographiques et Geochimiques, 15 rue Notre Dame des Pauvres, BP 20, 54501 Vandoeuvre lès Nancy, France.

[8] Glenn T. Seaborg Institute, Lawrence Livermore National Laboratory, Livermore, CA. 94550, USA.

[9] McDonnell Center for the Space Sciences, Department of Physics, Washington University, St. Louis, MO 63130, USA.

[10] School of Earth, Atmospheric and Environmental Sciences, The University of Manchester, Manchester, M13 9PL, UK.

[11] Museum National d'Histoire Naturelle, Laboratoire d'Etude de la Matiere Extraterrestre, 57 rue Cuvier, 75005, Paris, France.
[12] Division of Geological and Planetary Sciences, California Institute of Technology, Pasadena, CA 91125, USA.

[13] Max-Planck-Institute for Chemistry, Particle Chemistry Department, J.-J.-Becherweg 27, D-55128 Mainz, Germany.

[14] Robert M Walker Laboratory for Space Science, Astromaterials Research and Exploration Science Directorate NASA Johnson Space Center, Houston, TX 77058, USA.

[15] Department of Earth and Planetary Sciences, Harvard University, 20 Oxford Street, Cambridge, MA 02138.

[16] Impacts and Astromaterials Research Centre, Department of Mineralogy, Natural History Museum, Cromwell Road, South Kensington London, SW7 5BD, UK

[17] Sciences and Exploration Directorate, NASA Goddard Space Flight Center, Greenbelt, MD 20771, USA.

[18] ESCG/ Jacobs Sverdrup, Houston, TX 77058 USA.

[19] Department of Physics and Astronomy, Minnesota State University, 141 Trafton Science Center N, Mankato, MN 56001, USA

[20] School of Physics and Astronomy, University of Minnesota, 116 Church St. S. E., Minneapolis, MN 55455, USA

[21] Science Division, Jet Propulsion Laboratory, 4800 Oak Grove Drive, Pasadena, CA 91109 USA.

[22] Code 6360, Naval Research Laboratory, Washington, DC 20375

* to whom correspondence should be addressed. email: mckeegan@ess.ucla.edu

3193 words in text. 101 words in abstract.

Hydrogen, carbon, nitrogen, and oxygen isotopic compositions are heterogeneous among comet 81P/Wild2 particle fragments, however extreme isotopic anomalies are rare, indicating that the comet is not a pristine aggregate of presolar materials. Non-terrestrial nitrogen and neon isotope ratios suggest that indigenous organic matter and highly volatile materials were successfully collected. Except for a single circumstellar stardust grain, silicate and oxide minerals have oxygen isotopic compositions consistent with solar system origin. One refractory grain is ^{16}O-enriched like refractory inclusions in meteorites, suggesting formation in the hot inner solar nebula and large-scale radial transport prior to comet accretion in the outer solar system.

The isotopic compositions of primitive solar system materials record evidence of the chemical and physical processes involved in the formation of planetary bodies ~4.6 billion years ago and, in some cases, provide a link to materials and processes in the molecular cloud which predated our solar system. The vast majority of isotopic analyses of extraterrestrial materials have been performed on chondritic (undifferentiated) meteorites, which are samples of asteroids that likely accreted at 2-4 Astronomical Units (AU) within the first few million years of solar system history. Comets formed in much colder regions of the protoplanetary disk and are widely considered to consist of more primitive matter than even the most unequilibrated meteorites.

Analyses of isotope compositions of comets are rare. Measurements of D/H, $^{13}C/^{12}C$, $^{15}N/^{14}N$, or $^{18}O/^{16}O$ have been made for a few abundant molecules in gases of several comet comae by ground-based spectroscopy (*1-3*) and of comet P/Halley by mass spectrometers on the Giotto spacecraft (*4*). The nitrogen isotope measurements indicate heterogeneity between precursor molecules of different coma gases (*3*), presumably reflecting a contribution from isotopically heavy refractory organics. Direct measurements of isotope compositions in the dust fraction of comets are limited to low precision data from the Halley flyby (*5*). Isotopic measurements of stratosphere-collected interplanetary dust particles (IDPs) demonstrate the highly primitive nature of many

anhydrous IDPs (e.g., *6, 7, 8*), however a cometary origin for specific individual particles cannot be ascertained. Here, we report laboratory analyses of the light 'stable' isotopes of H, C, N, O, and Ne in individual grains, particle fragments, crater debris, and/or trapped volatile materials collected from comet 81P/Wild2 and returned to Earth by the NASA Discovery Mission, STARDUST (*9*).

The goals of the Isotope Preliminary Examination Team analyses are to provide first-order answers to questions relating to the provenance of Wild2 dust: 1) does the comet consist of a mechanical agglomeration of essentially unprocessed, or perhaps only thermally-annealed, presolar materials? 2) do comets provide a well-preserved reservoir of circumstellar dust grains (*10*) with distinct nucleosynthetic histories (i.e., stardust)? 3) can isotopic signatures establish whether extraterrestrial organic materials are present in the aerogel collection medium above contamination levels? 4) what are the relationships to known isotope reservoirs in meteoritic samples and in IDPs? 5) what are the implications for mixing and thermal processing in the early solar system? The Preliminary Examination has focused on the abundant light elements H, C, N, O and light noble gases because they have characteristic isotopic signatures that vary widely in solar system materials (e.g., *11*), and these compositions often can be linked to distinct astrophysical environments and/or processes (*12*).

Hydrogen isotopic compositions in fragments of five Wild2 particles extracted from aerogel range from values similar to terrestrial and chondritic, up to moderate D/H enhancements of ~3× the D/H in mean ocean water (Fig. 1, Table S1), with a few 'hotspots' up to a maximum $\delta D = 2200 \pm 900‰$ (*13*). All observed D enrichments are associated with carbon although only one of the samples (T17) is dominated by carbonaceous material without intermixed silicates. While overlapping the range of values observed for IDPs (*14-16*) and water in (Oort cloud) comets (*4*), the maximum D/H is well below that characteristic of a minor component of organic matter in anhydrous IDPs, especially of the low-density 'cluster' type thought to be derived from comets (*17*). The maximum D/H values of Wild2 grains are also far less than those measured in small 'hotspots' of insoluble organic matter separated from carbonaceous chondrites (*18*) and in cometary HCN ice (*19*), which are both thought to have close affinities to organic material produced at very low temperatures in molecular cloud

environments. Because only a few samples have so far been investigated, we cannot conclude that this relative paucity of highly D-enriched matter signifies an intrinsic difference between Wild2 samples and macromolecular materials in IDPs and carbonaceous chondrites. It is also possible that the D/H signatures were modified by alteration/contamination during impact. Although the particles so far investigated are not rich in carbon, with the one noted exception, and most have D/H values similar to that of cometary water, there is no evidence that the Wild2 particles contain any phyllosilicate minerals; thus it cannot be argued that the D/H values are sampling Wild2 water.

Some cometary volatiles do appear to have been captured by the aerogel. Helium, neon, and argon abundances, as well as $^{20}Ne/^{22}Ne$ ratios, were analyzed in two bulbous sections of an impact track that contains fragments of fine-grained impactor material mixed with melted aerogel along its periphery. Noble gases in a control sample (unexposed aerogel taken from the rear portion of a collector cell) are consistent with system blanks, indicating that flight aerogel does not contain any detectable background of noble gases. In contrast, aerogel fragments containing the impact track show excess He and Ne above blank levels by factors of 3 to 4 (Table S2). Either the impacting particles altered the aerogel in such a way as to make it more prone to preserving atmospheric contamination during vacuum degassing, or the very rapid timescales ($<\mu$sec) for melting of aerogel during deceleration of comet particles helped trap indigenous cometary volatiles. Evidence from Ne isotope ratios points toward the latter interpretation. Although gas amounts are small ($\sim 10^{-15}$ mole), requiring significant blank corrections, $^{20}Ne/^{22}Ne = 10.14 \pm 0.12$, which is higher than that in air by $\sim 3\sigma$. In a $^{22}Ne/^{20}Ne$ versus $^{4}He/^{20}Ne$ diagram (Fig. S1), the data do not lie on a pure mixing trajectory between air and the solar composition but instead point toward a non-atmospheric endmember with a $^{4}He/^{20}Ne$ ratio lower than solar, which is consistent with expectations for comets due to preferential trapping of heavier noble gases in ice accreted at ~30K (*20*).

All carbon and nitrogen isotope analyses were made by isotopic mapping with NanoSIMS instruments by measuring atomic ions of C^- and isotopologs of the intense CN^- beam, respectively. Microtomed particles extracted from aerogel as well as Al-foil crater debris were mapped with a spatial resolution of ~100 nm to search for isotopic

anomalies that could identify circumstellar dust grains like the rare carbide and nitride phases (SiC, Si_3N_4, graphite) found in primitive meteorites (*21*). No circumstellar dust grains were definitively identified despite an intensive search comprising more than 20 slices and fragments from a dozen particles and ~5700 μm^2 of debris in and around 6 small (< 2 μm) and 4 large (> 50 μm) craters on Al-foil collectors. This result is in contrast to inferences of a population of nearly pure ^{12}C grains in comet Halley (*5*). One ~150 nm region has an isotopic composition ($\delta^{13}C = 59\pm61$; $\delta^{15}N = -518\pm6$) which falls in a range consistent with 'mainstream' presolar SiC grains (*21*), however the grain was sputtered away before a mineral identification could be made. Another "hotspot" was enriched in ^{13}C ($\delta^{13}C = 964\pm219$‰) and depleted in ^{15}N ($\delta^{15}N = -415\pm94$‰), typical of mainstream SiC, however the ion emission area was not as localized as would be expected for a very small circumstellar grain and, moreover, it had a high abundance of nitrogen (inferred C/N ~3). This grain disappeared rapidly under ion bombardment as did a second spot with a low inferred C/N ratio ≈ 6 and low $\delta^{15}N \approx -350$‰. This behavior is consistent with sputtering of labile organic material. In fact, labile organic matter has been identified in the aerogel by several molecular spectroscopic methods (Sandford et al., this volume) and the successful capture of highly volatile organic compounds is qualitatively consistent with the retention of some cometary noble gases. Interestingly, this isotopically light nitrogen component is only rarely seen in IDPs (*8, 22*), but within ~10% uncertainties, it is consistent with estimates of the nitrogen isotopic composition in HCN gas from comet Hale Bopp (*23*) and of the solar composition based on analyses of the Jovian atmosphere (*24*) and of solar wind implanted in lunar grains (*25*).

On the scale of a few microns, all samples are homogeneous in both C and N isotope compositions and show no correlation between $\delta^{13}C$ and $\delta^{15}N$ (Fig. 2). Carbon isotopes fall in a particularly restricted range with most "bulk" $\delta^{13}C$ values falling between −20 and −50‰. This range is somewhat higher than recent estimates ($\delta^{13}C = -105\pm20$‰) for the solar carbon isotope composition (*26*), but it is compatible with carbon isotopes in other primitive solar system matter including IDPs (*17, 27*) and most organic matter in chondrites (*28, 29*).

A wider range is observed for "bulk" nitrogen with many samples clustering near 0‰ (atmospheric), but others showing modest $\delta^{15}N$ enrichments of ~+100 up to ~+500‰, similar to the range observed for anhydrous IDPs (*30*). On a sub-micron scale, more extreme values are found with a maximum observed $\delta^{15}N \sim +1300\pm400$‰, which is similar to the highest values found in refractory organic matter in IDPs (*8*) and meteorites (*18*). Unlike IDPs, however, at this fine spatial scale the Wild2 samples display both low and high $\delta^{15}N$, indicating an unequilibrated mixture of a low $\delta^{15}N$ (perhaps icy) component and a more refractory (high C/N) organic material that has high $\delta^{15}N$ and isotopically 'normal' carbon. The fact that most IDPs are typically characterized by ^{15}N excesses (compared with air) may reflect the instability of the more labile low $\delta^{15}N$ component during atmospheric entry heating. Thus the Wild2 samples could represent a fundamentally different type of organic material than that which is available for study through the stratospheric IDPs, although it is puzzling that the Wild2 particles analyzed thus far appear to be relatively deficient in total organic matter (compared to most IDPs) based on low signals for C^- and CN^-. This observation contradicts expectations of comets as being very rich in organic matter, and may indicate that much of the Wild2 organic matter did not survive the capture process as discrete phases still closely associated with silicate minerals.

Oxygen is the most abundant element in rocky planets, asteroids, and comets, and for reasons that are not yet understood (*31*), it exhibits distinctive isotopic compositions that are essentially unique to each class of planetary materials from the inner solar system for which we have samples (*32*). Although the isotopic variations that occur on planetary scales are relatively subtle (less than a few ‰), individual components of unequilibrated meteorites that formed in the solar nebula (e.g., refractory Ca-Al-rich inclusions or CAIs, chondrules, fine-grained olivine in CAI rims or in matrix) can have oxygen isotope compositions that vary by 50‰ or more in their relative abundances of ^{16}O (e.g., *11*). These isotopic variations are fairly systematic (*33*) and, together with the planetary scale variations, imbue oxygen with a unique diagnostic capability to indicate provenance of a suite of samples (*34*). Orders of magnitude greater isotopic variations are observed in presolar oxide and silicate dust grains which condensed in the outflows of evolved, mass-losing stars and inherited specific isotopic compositions due to local nucleosynthetic

processes (*35*). Large isotopic anomalies in oxygen have been used to identify presolar silicate minerals and amorphous silica-rich components in anhydrous stratospheric IDPs (*7*). Little definitive data exist regarding oxygen isotope compositions in cometary materials. In situ measurements of water ice from comet Halley, made by the *Giotto* mission, yield $\delta^{18}O = 12\pm75‰$ (*4, 36*) but no measurement of $\delta^{17}O$ is available.

Oxygen isotope measurements of Wild2 samples were made by mapping techniques to search for presolar grains and by focused probe SIMS on individual particle fragments to relate the comet samples to known classes of meteoritic materials (SOM). Of some two dozen particle fragments prepared as microtomed (<200 nm thick) sections from aerogel keystones (*37*), no candidate presolar grains were identified on the basis of extreme oxygen isotope anomalies (defined as >20% or 4σ removed from terrestrial values). For many samples, the measurement of oxygen isotopes was compromised by mixing with melted aerogel, which could not be resolved even with the <100 nm spatial resolution of the NanoSIMS. For this reason, residues from impact craters in the Al-foil targets (Horz et al, this volume) were also examined by high resolution isotope mapping.

Thirty-seven small craters, between 320 nm and 1.5 μm diameter, and 4 large craters (59, 72, 140, and >200 μm) were mapped, resulting in the identification of ~10^4 O-rich grains or sub-areas in the ion images. Only one presolar grain was found (Fig. 3). The ~250 nm grain is highly enriched in ^{17}O and slightly depleted in ^{18}O compared to solar system samples and has a composition of $^{17}O/^{16}O = (1.01\pm0.20)\times10^{-3}$ and $^{18}O/^{16}O = (1.77\pm0.24)\times10^{-3}$. This isotopic composition is typical for presolar oxide (and silicate) grains belonging to 'group 1', thought to originate in red giant or asymptotic giant branch stars (*35*). Unfortunately, the mineralogy of the grain could not be determined (*38*), although it is likely that it was a relatively refractory oxide or silicate as it could not have retained its distinctive oxygen isotopic composition if it had been vaporized/recondensed or even melted appreciably during impact.

High precision oxygen isotope measurements were made in 5 to 10 μm spots of individual "terminal grains" separated from aerogel tracks and pressed into clean Au foil. Fragments from one enstatite-rich grain (T69) and one forsterite-rich grain (T22) have similar oxygen isotope compositions that plot slightly below the terrestrial mass fractionation (TF) line and to the low $\delta^{18}O$ side of the ^{16}O-mixing line that characterizes

refractory components (CAIs) in chondrites (Fig. 4; Table 2 SOM). Analyses of other grains (not shown in Fig. 4, but presented in the SOM) that were heavily contaminated by adhering aerogel (or acrylic embedding medium) plot toward the TF line at very negative $\delta^{18}O$ (~ −20 ‰) reflecting strong instrumental mass fractionation. Although unlikely, we cannot exclude the possibility that the deviation of the T69 and T22 data from the CAI mixing line is due to a minor contamination with aerogel (*39*). In any case, the oxygen isotopic compositions of these Mg-rich silicates from Wild2 are compatible with those of most mafic silicate minerals from carbonaceous chondrite chondrules.

Oxygen isotopes were also measured in a polymineralic refractory grain (T25, "Inti") using both NanoSIMS mapping and higher precision ims 1270 spot measurements (SOM). The sample consists of a fine-grained mix of spinel, Al-rich diopside, melilite, anorthite, with minor perovskite (see Zolensky et al., this volume). Although the NanoSIMS analyses resolve individual phases, it was not possible to avoid sampling multiple mineral phases during the ims 1270 analyses (5 μm diameter spot). The data are, however, all consistent (Fig. 4) demonstrating that the sample is isotopically homogeneous (*40*) with a composition that is ^{16}O-rich compared to most planetary materials ($\delta^{18}O \approx \delta^{17}O \approx -40‰$). Remarkably, this composition is virtually identical to that of a large population of CAIs and refractory oxide grains in chondrites (e.g., *11, 41, 42*), although it does not represent an extreme ^{16}O-rich "end-member" composition for solar system materials (*43*). Similarly ^{16}O-enriched compositions have been observed for rare refractory IDPs collected in the stratosphere (*44, 45*), but the nature of the relationship between these particles and meteoritic CAIs has not been thoroughly investigated.

As an ensemble, the isotopic compositions of the abundant light elements demonstrate that the dust of comet Wild2 is an unequilibrated aggregation of materials from different astrophysical sources. The H, C, and N isotope compositions indicate the presence of several minor components which are isotopically fractionated to large degrees, probably reflecting chemical reactions at very low temperatures like those characteristic of molecular cloud or, possibly, Edgeworth-Kuiper belt environments. This is consistent with a general view of Jupiter Family comets as having accreted from cold materials at the edge of the solar nebula. In contrast, two observations run counter

to expectations: 1) based on C, N, and O isotopes, the abundance of presolar grains appears to be low compared to primitive meteorites and IDPs, and 2) the comet contains high-temperature silicate and oxide minerals with oxygen isotopic compositions essentially identical to those of analogous minerals in carbonaceous chondrites. The first observation could perhaps be explained as a preservation effect, however the one presolar grain firmly identified was found in the residue of the largest impact crater so far investigated (which actually punctured a hole through the Al-foil). If similar grains were abundant, they would likely have been seen in or around other craters and in the aerogel as well. It could be argued that if most of the presolar materials making up the comet's dust consisted not of circumstellar grains but rather of interstellar amorphous silicates, they would either have suffered too much mixing with aerogel, or, in the case of residue in Al-foil craters, they might never have possessed sufficiently anomalous oxygen isotopic compositions to be recognized as non-solar. These possibilities cannot be ruled out at this preliminary stage of the investigation. However, such ambiguity is not permitted by the second constraint.

The crystalline silicate and oxide minerals for which we have oxygen isotope data could not have formed by annealing (devitrification) of presolar amorphous silicates in the Kuiper belt. Not only is such an origin incompatible with the chemistry and mineralogy of these grains, but, in addition, the fact that these grains differ markedly in their relative ^{16}O abundances demonstrates that they could not have formed from a single isotopic reservoir. It is not known if the compositions of any of these samples is close to solar (*46*), but the similarity in O-isotope composition between Wild2 grains and materials from carbonaceous chondrites which clearly formed in the inner solar system (<5 AU) is striking. Identifying precisely what regions of the inner solar system may be sampled by this comet is clearly very important to understanding the scale of radial mixing outward in the solar protoplanetary disk.

Most interstellar silicate dust is thought to be amorphous (*47*) and with recent recognition of the relatively large fraction of crystalline silicates in comets and in protostellar disks based on infrared spectral data (e.g., *48*), astronomers have postulated mixing of dust from inner warm regions, where ambient conditions are above glass transition temperatures, outward to Kuiper belt regions (e.g., *49, 50*). However, other

observations suggest production of crystalline silicates (specifically forsterite) at large (>10 AU) stellar distances (*51*). That the CAI-like particle ("Inti") has the same intrinsic oxygen isotopic properties as CAIs from all major classes of primitive meteorites (*42, 52, 53*), argues strongly for an origin in the same source region as meteoritic CAIs. One possibility is that this region (*54*) could be at the inner truncation of the accretion disk (<0.1 AU) where very high temperatures exist. Here winds associated with bi-polar outflows, driven by interactions of the young Sun with the accretion disk, can carry small refractory particles to large heliocentric distances where they can accrete together with cold, icy materials (*55, 56*). Other models (*57*) invoke turbulent transport of hot inner nebula (silicate) dust out to zones of comet accretion which could account for the carbonaceous chondrite-like isotopic compositions of Wild2 olivine and pyroxene grains. We conclude that the coupled oxygen isotope and mineralogic data are best understood as indicating that a significant fraction of dust in comet Wild2 is derived from chemically and thermally processed precursors from the inner solar system, consistent with predictions of the X-wind and other models (*55-57*) for the protosolar disk.

This work was performed under the auspices of the U. S. Department of Energy by University of California, Lawrence Livermore National Laboratory under contract W-7405-Eng-48.

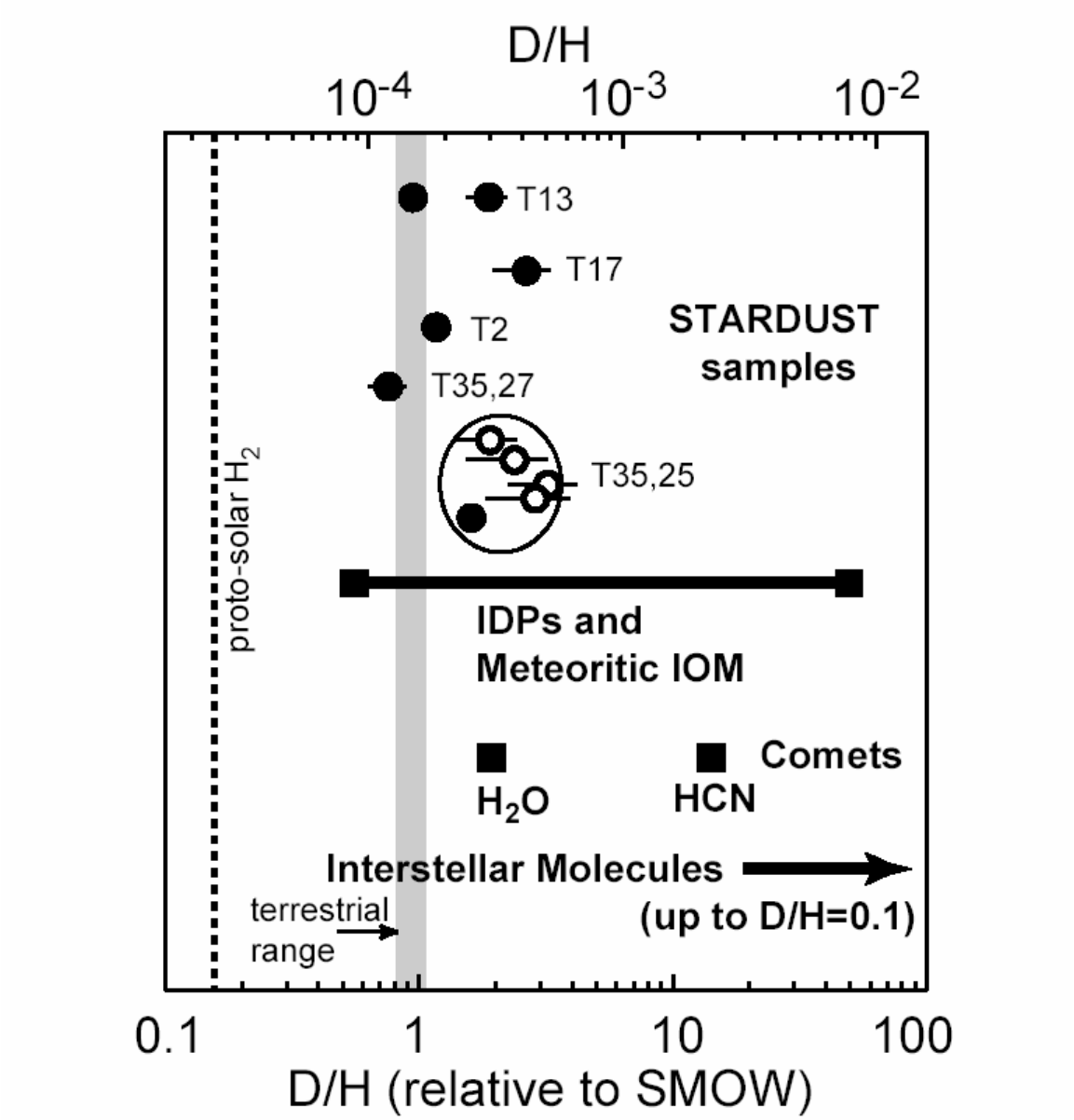

Figure 1. Hydrogen isotopic compositions in bulk fragments (solid circles) of 5 Wild2 particles and in micron-sized sub-areas of one particle (open circles) compared to Standard Mean Ocean Water (SMOW) and to ranges of laboratory measurements of D/H in stratosphere-collected Interplanetary Dust Particles (IDPs) and in Insoluble Organic Matter (IOM) from chondritic meteorites. Also shown are an estimate for protosolar H_2 and ranges of D/H measured remotely for specific gaseous molecules from comets and for molecular clouds. Error bars on STARDUST samples are 1σ.

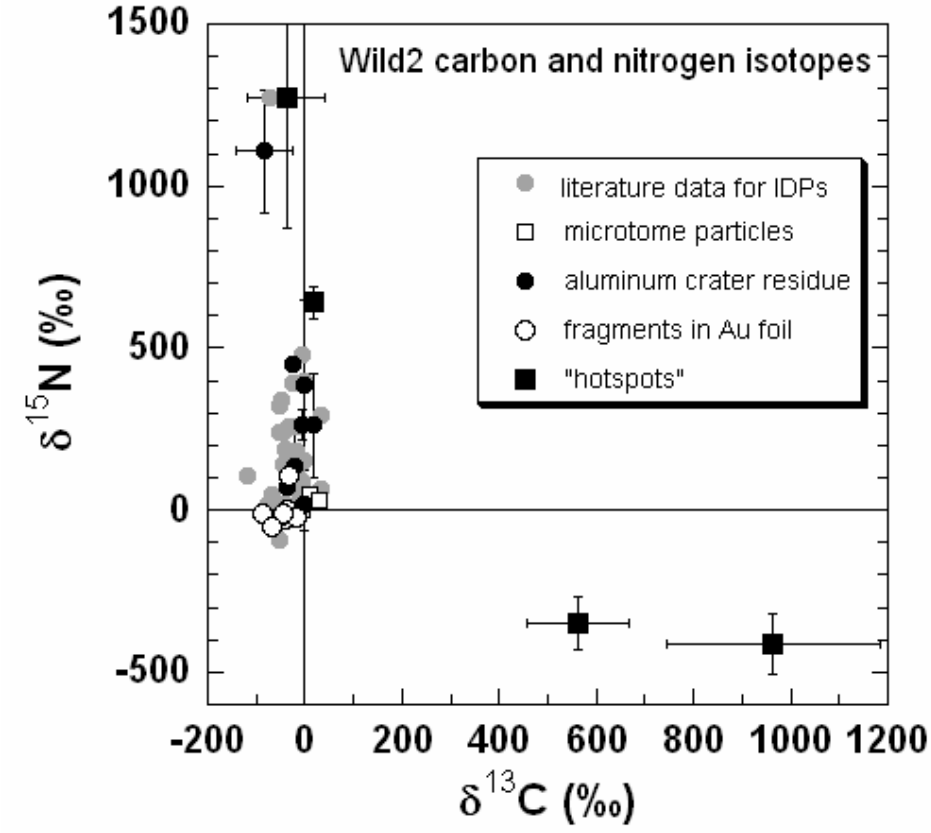

Figure 2. Correlated carbon and nitrogen isotopic compositions of individual cometary grains compared to literature data (grey circles) for stratosphere-collected IDPs (*8,22*). All data were collected by isotope mapping with NanoSIMS instruments. Shown are average values for cometary grains prepared as microtome sections (open squares), for fragments extracted from aerogel and pressed into Au foil (open circles), and for residue in and surrounding craters in the Al foil collector (solid circles). Also shown are selected "hotspots" (solid squares) from the crushed samples. A low $\delta^{15}N$ component is seen in hotspots with low inferred C/N values, possibly reflecting labile organic materials. Except for these hotspots, the Wild2 samples exhibit a relatively narrow range in $\delta^{13}C$ and enrichments in $\delta^{15}N$ that match well with the range previously observed in IDPs.

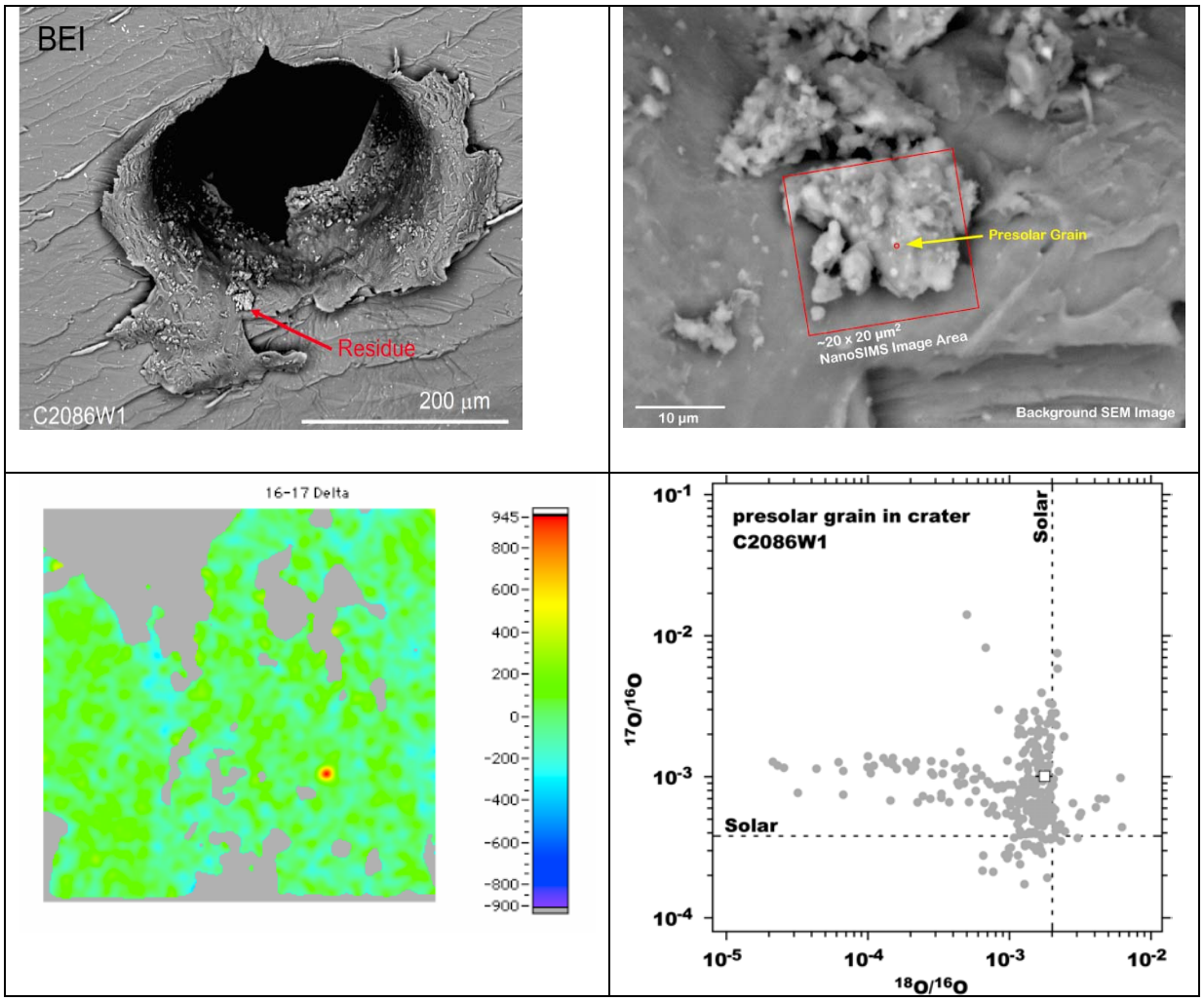

Figure 3. Presolar grain in residue of crater C2086W1. top left: Backscattered electron image of crater which punctured Al-foil; top right: electron image of projectile residue in crater lip (scale bar = 10 µm); bottom left: 20 × 20 µm false color isotope map of $\delta^{17}O$ measured by high resolution NanoSIMS; bottom right: oxygen 3 isotope plot of presolar grain (open square) compared to literature data for presolar oxide grains separated from meteorites. On this scale, all materials formed in the solar system plot at the intersection of the two dashed lines.

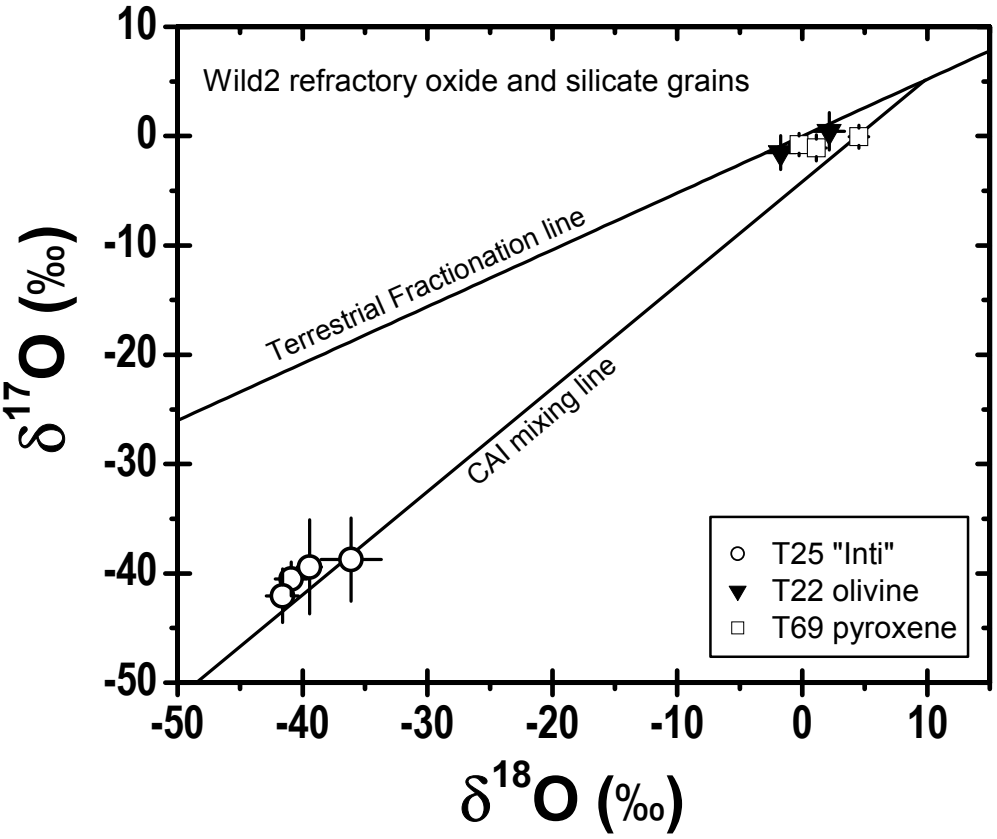

Figure 4. Oxygen isotopic compositions of individual cometary grains. Shown are 4 measurements of T25, a refractory mineral assemblage consisting primarily of spinel, Al-diopside, melilite, and anorthite, with accessory osbornite and perovskite. Also shown are measurements of fragments of T22, an Mg-rich olivine grain, and T69, a Mg-rich pyroxene. T25 is ^{16}O-enriched to a level similar to that seen in many CAIs, whereas T22 and T69 have compositions similar to mafic silicate minerals in carbonaceous chondrites. Error bars are 2σ.

References and Notes

1. D. Hutsemekers *et al.*, *Astronomy & Astrophysics* **440**, L21 (Sep, 2005).
2. E. Jehin *et al.*, *Astrophysical Journal* **613**, L161 (Oct 1, 2004).
3. C. Arpigny *et al.*, *Science* **301**, 1522 (Sep 12, 2003).
4. P. Eberhardt, M. Reber, D. Krankowsky, R. R. Hodges, *Astronomy and Astrophysics* **302**, 301 (Oct, 1995).
5. E. K. Jessberger, *Space Science Reviews* **90**, 91 (1999).
6. S. Messenger, F. J. Stadermann, C. Floss, L. R. Nittler, S. Mukhopadhyay, *Space Science Reviews* **106**, 155 (2003).
7. S. Messenger, L. P. Keller, F. J. Stadermann, R. M. Walker, E. Zinner, *Science* **300**, 105 (Apr 4, 2003).
8. C. Floss *et al.*, *Geochimica et Cosmochimica Acta* **70**, 2371 (May, 2006).
9. P. Tsou *et al.*, *Journal of Geophysical Research-Planets* **109** (Dec 22, 2004).
10. We differentiate, in principle, between different types of presolar materials: "circumstellar" dust grains formed as condensates in the ejecta of evolved stars – hence they are literally stardust – whereas presolar dust also includes dust particles which formed or were reprocessed in the interstellar medium. In practice, it is not clear if the latter could be recognized solely on the basis of isotopic compositions (given that radiometric dating is not yet possible).
11. K. D. McKeegan, L. A. Leshin, *Stable Isotope Geochemistry* **43**, 279 (2001).
12. A wide variety of Wild2 sample types have been probed by several analytical tools to provide a preliminary characterization of the range of isotope effects present. Spot analyses of H, C, N, and O isotopes were performed by secondary ion mass spectrometry (SIMS) on entire particle fragments (typically ~2 – 10 μm) extracted from aerogel collector blocks and pressed into clean gold foil. Such "bulk" analyses tend to yield the highest precision, but may average over any isotope heterogeneities existing on a very fine spatial scale, and in some cases, also suffer from contamination by compressed aerogel adhering to the periphery or even intimately mixed with the comet particle. Data on whole particle fragments are suitable for comparison to spectroscopic data (IR, Raman) acquired with similar resolution and with mineralogy/petrology at the scale of the scanning electron microscope. Much higher spatial resolution is achieved by NanoSIMS analysis, which uses a primary ion beam <100 nm in diameter rastered over the sample surface to produce elemental and isotopic "maps". NanoSIMS analyses typically realize worse precision but clearly discriminate against aerogel contamination and can also be used to identify sub-micron circumstellar dust grains amidst more normal (i.e., solar system-like) materials by virtue of their potentially large isotope anomalies.
13. the delta notation expresses the relative deviation of a measured composition from that of a standard reference material in parts per thousand. Thus, $\delta D = [(D/H)_{sample}/(D/H)_{standard} -1]\times 1000$ and similarly for $\delta^{13}C$, $\delta^{15}N$, and $\delta^{17}O$, etc. The conventional reference standards are used here: standard mean ocean water (SMOW) for H and O, PDB for C, and air for N. Absolute values for these standards are defined as $(D/H)_{SMOW} = 1.556\times 10^{-4}$; $(^{18}O/^{16}O)_{SMOW} = 2.0052\times 10^{-3}$; $(^{17}O/^{16}O)_{SMOW} = 3.8288\times 10^{-4}$; $(^{13}C/^{12}C)_{PDB} = 1.12372\times 10^{-2}$; $(^{15}N/^{14}N)_{AIR} =$

3.6765×10^{-3}. Unless noted, uncertainty estimates reported in this paper are 2σ (standard error).
14. K. D. McKeegan, R. M. Walker, E. Zinner, *Geochimica et Cosmochimica Acta* **49**, 1971 (1985).
15. S. Messenger, R. M. Walker, in *Astrophysical implications of the laboratory study of presolar materials, AIP Conf. Proc.* T. J. Bernadowicz, E. K. Zinner, Eds. (American Institute of Physics, St. Louis, 1997), vol. 402, pp. 545-564.
16. J. Aléon, C. Engrand, F. Robert, M. Chaussidon, *Geochimica et Cosmochimica Acta* **65**, 4399 (2001).
17. S. Messenger, *Nature* **404**, 968 (2000).
18. H. Busemann *et al.*, *Science* **312**, 727 (May, 2006).
19. R. Meier *et al.*, *Science* **279**, 1707 (1998).
20. A. Bar-Nun, T. Owen, in *Solar System Ices* B. B. Schmidt, C. De Bergh, M. Festou, Eds. (Kuwer Acad., Norwell, Mass., 1998) pp. 353-366.
21. D. D. Clayton, L. R. Nittler, *Annual Review of Astronomy and Astrophysics* **42**, 39 (2004).
22. J. Aleon, F. Robert, M. Chaussidon, B. Marty, *Geochimica et Cosmochimica Acta* **67**, 3773 (Oct, 2003).
23. D. C. Jewitt, H. E. Matthews, R. Meier, *Science* **278**, 90 (1997).
24. T. Owen, T. Encrenaz, *Space Science Reviews* **106**, 121 (2003).
25. K. Hashizume, M. Chaussidon, B. Marty, F. Robert, *Science* **290**, 1142 (2000).
26. K. Hashizume, M. Chaussidon, B. Marty, K. Terada, *Astrophysical Journal* **600**, 480 (Jan, 2004).
27. F. J. Stadermann, R. M. Walker, E. Zinner, *Meteoritics* **24**, 327 (1989).
28. F. Robert, S. Epstein, *Geochimica et Cosmochimica Acta* **46**, 81 (1982).
29. J. F. Kerridge, *Geochimica et Cosmochimica Acta* **49**, 1707 (1985).
30. C. Floss *et al.*, *Science* **303**, 1355 (Feb, 2004).
31. The origin of this pervasive isotopic anomaly is currently thought to be related to either isotope selective photochemistry (*58-60*), or to kinetic effects based on symmetric vs. asymmetric isotopologs for reactions in the gas phase (*61*) or on grain surfaces (*62*).
32. R. N. Clayton, *Annual Review of Earth and Planetary Sciences* **21**, 115 (1993).
33. for example, CAIs are nearly always enriched in ^{16}O compared to chondrules, and carbonaceous chondrite materials are more ^{16}O-enriched than their petrologically similar counterparts (chondrules, matrix, etc.) in ordinary chondrites.
34. in fact, oxygen isotope composition is a critical parameter for meteorite classification and has been used to identify meteorites from Mars and from the Moon (*32*).
35. L. R. Nittler, in *Astrophysical Implications of the Laboratory Study of Presolar Materials* T. J. Bernatowicz, E. K. Zinner, Eds. (American Inst. Physics, Woodbury, 1997) pp. 59-82.
36. H. Balsiger, K. Altwegg, J. Geiss, *JGR* **100**, 5827 (1995).
37. A. J. Westphal *et al.*, *Meteoritics & Planetary Science* **37**, 855 (Jun, 2002).
38. Following the isotopic measurements, focused ion beam (FIB) methods were used to cut the Al-foil in order to expose a cross section containing the presolar grain. Unfortunately, the ~300 nm grain was not found in a reanalysis in the NanoSIMS, indicating that the FIB cut missed its target. As the FIB kerf is many times larger

than the grain diameter, location of the cut is critical and sometimes difficult in heterogeneous samples.
39. NanoSIMS data, obtained on ~0.5 mm fragments of grains from T69 and T22, are devoid of any aerogel contamination (due to the fine primary beam diameter) and generally corroborate the "bulk" analyses but within a precision of ~20‰.
40. "matrix effects" in the instrumental mass fractionation are known to be small for this suite of minerals.
41. R. N. Clayton, T. K. Mayeda, *Earth and Planetary Science Letters* **67**, 151 (1984).
42. K. D. McKeegan, L. A. Leshin, S. S. Russell, G. J. MacPherson, *Science* **280**, 414 (1998).
43. K. Kobayashi, H. Imai, H. Yurimoto, *Geochemical Journal* **37**, 663 (2003).
44. K. D. McKeegan, *Science* **237**, 1468 (1987).
45. M. E. Zolensky, *Science* **237**, 1466 (1987).
46. Unfortunately, the oxygen isotopic composition of the Sun is not known with any reasonable precision, and estimates based on analyses of a surface correlated component in lunar metal grains vary by at least 10% (*63,64*).
47. F. Kemper, W. J. Vriend, A. Tielens, *Astrophysical Journal* **609**, 826 (Jul, 2004).
48. F. Molster, C. Kemper, *Space Science Reviews* **119**, 3 (Jul, 2005).
49. J. Bouwman *et al.*, *Astronomy & Astrophysics* **375**, 950 (Sep, 2001).
50. R. van Boekel *et al.*, *Nature* **432**, 479 (Nov, 2004).
51. J. Bouwman, A. de Koter, C. Dominik, L. Waters, *Astronomy & Astrophysics* **401**, 577 (Apr, 2003).
52. T. J. Fagan, K. D. McKeegan, A. N. Krot, K. Keil, *Meteoritics & Planetary Science* **36**, 223 (2001).
53. Y. Guan, K. D. McKeegan, G. J. MacPherson, *Earth and Planetary Science Letters* **183**, 557 (Dec 15, 2000).
54. Evidence from short-lived radioisotopes (*65, 66*) supports formation of CAIs in X-wind type scenarios which link bi-polar outflows to high particle radiation environments. Oxygen isotope considerations also favor formation of CAIs in a restricted nebula locale (*67*), but this also implies a different source region for more isotopically "normal" silicate minerals.
55. K. Liffman, M. Brown, *Icarus* **116**, 275 (Aug, 1995).
56. F. H. Shu, H. Shang, T. Lee, *Science* **271**, 1545 (Mar 15, 1996).
57. D. Bockelée-Morvan, D. Gautier, F. Hersant, J. M. Huré, F. Robert, in *Astronomy and Astrophysics*. (2002), vol. 384, pp. 1107-1118.
58. R. N. Clayton, *Nature* **415**, 860 (2002).
59. J. R. Lyons, E. D. Young, *Nature* **434**, 317 (2005).
60. H. Yurimoto, K. Kuramoto, *Science* **305**, 1763 (2004).
61. M. H. Thiemens, *Science* **283**, 341 (1999).
62. R. A. Marcus, *The Journal of Chemical Physics* **121**, 8201 (2004).
63. K. Hashizume, M. Chaussidon, *Nature* **434**, 619 (Mar 31, 2005).
64. T. R. Ireland, P. Holden, M. D. Norman, *Geochimica et Cosmochimica Acta* **69**, A382 (May, 2005).
65. K. D. McKeegan, M. Chaussidon, F. Robert, *Science* **289**, 1334 (2000).
66. M. Chaussidon, F. Robert, K. D. McKeegan, *Geochimica et Cosmochimica Acta* **70**, 224 (Jan 1, 2006).

67. A. N. Krot, K. D. McKeegan, L. A. Leshin, G. J. MacPherson, E. R. D. Scott, *Science* **295**, 1051 (2002).

Supporting On-line Material

Hydrogen isotopic measurements

Hydrogen isotopes were measured along with carbon using a Cameca ims-6f ion microprobe at the Carnegie Institution of Washington, in scanning imaging mode. A focused <10pA Cs^+ ion beam was rastered across samples with synchronized collection of secondary ions. Techniques were identical to those described in {Busemann, 2006 #1767}. All but one analyzed sample were extracted from the aerogel collectors and pressed into Au foils. A 500 nm thick slice of sample Track 13 (FC9,0,13,1,0) prepared by ultramicrotome, was placed directly on a Au foil. Data were quantified using custom image processing software and terrestrial standards.

Table S1. D/H ratios measured in Stardust samples (1σ errors)

Sample	δD/H (‰)	D/H ($\times 10^6$)
Track 13	900±350	296±55
Track 35,25 (bulk)	633±119	254±19
Sub-region	1899±1057	451±165
Sub-region	2243±984	505±153
Sub-region	1394±839	373±131
Sub-region	917±542	299±84
Track 35,27	-238±130	119±20
Track 2	176±115	183±18
Track 17	1655±676	413±105

Noble gas analysis of bulbous particle tracks in Stardust aerogel: a seach for cometary volatiles

Noble gases were measured in blank aerogel chips, flown aerogel chips and two fragments of bulbous aerogel at the CRPG in Nancy, France. The first piece had material from the wall of a large bulbous track (c2044,0,41; tile 44, track 7; hereafter, "Thera1"). This sample together with blank and flown samples were analysed during a first session on 12-15 June, 2006 after extensive blank determination. Given the results of this first trial, we were supplied with a second, larger, piece of the same wall, referred here as "Thera 2". This sample was analysed together with another piece of flown aerogel on 11-13 July, 2006.

Samples were handled in a clean room (class 10,000 in the room, class 100 in extraction boxes) under a microscope using a clean single-hair paintbrush attached to a manipulator. It was not possible to weigh aerogel chips due to their small size, and we have estimated the mass from optical measures of the surface area of the chips (assuming that all chips have a comparable thickness). Samples were loaded in pits of the laser chamber and connected to a high vacuum line developed for the analysis of ET samples. Samples were outgassed at 80°C (Thera 1 run) and 100°C (Thera 2 run) overnight and left pumping (1.5×10^{-9} mbar) at room temperature for 3 weeks (Thera 1) and 1 week (Thera 2).

Chips were heated using a CO_2 infrared (λ = 10.6 μm) laser mounted on a x-y stage and monitored through a microscope equipped with a CCD camera. A visible (He-Ne) laser was used to align the IR laser and we discovered that even the weak pointer laser was provoking vibrations of the chips under illumination. Hence we heated the

chips with great care by increasing very slowly the power of the CO_2 laser in order to avoid sample jumping out of the pits. We lost one blank aerogel sample and thus we did not analyse other small blank aerogel samples. Fortunately, the flown aerogel chips and the bulbous chips were bigger and could be safely analysed. Once thermal coupling of the aerogel sample with the laser beam was achieved, aerogel chips could be totally molten. Gases were purified over two titanium getters and analysed with a VG5400 static mass spectrometer following methods presented elsewhere [*Marty et al.*, 2005]. Analytical blanks (without laser heating and with laser heating of a metal surface adjacent to the samples) were thoroughly investigated and analyses started only when the blanks were indistinguishable to those of the purification line alone, as determined during several months prior to these experiments. The blanks (n= 6) were 4.9±2.9 x 10^{-15} mol, 0.86±0.20 x 10^{-15} mol, and 0.11±0.03 x 10^{-15} mol for ^{4}He, ^{20}Ne and ^{36}Ar, respectively (Table 1).

Results (Table S2) suggest that aerogel chips containing bubbles and cometary particle fragments have excesses of helium and neon relative to the blanks. For argon, all measurements were within the range of blank values and are not discussed further. We found no relationship between the aerogel surface area and the amount of extracted gas, for both helium and neon. Extractions of flown aerogel without bubbles are comparable to the blanks, given uncertainties. This suggests strongly that the instrumental blank dominates over the aerogel blank for the sample size we analysed. Therefore, an upper limit of the aerogel blank is given by instrumental blanks (Table S2).

Both Thera 1 and Thera 2 show excesses of He and Ne relative to blank levels. A possible exception is helium extracted from Thera 2 which is close to the amount of He extracted from the unexposed flight aerogel #1. Unfortunately, ^{3}He could not be analysed with confidence due to the low He amount and the mass spectrometer setting, which was a compromise (trap current of 200 μA, electron energy of 65 eV) made to analyse He, Ne and Ar together.

Data reduction for Ne isotopic ratios required correction for significant blank contribution, which was done by subtracting from either Thera 1 or Thera 2 data the respective flown aerogel (runs #1 & #2). When propagating errors, we considered that standard deviations of repeated blank measurements were representative of blank correction uncertainties and adopted these as errors on blank measurements. During the Thera 1 run, the analyser electronics had a drift problem which resulted in increasing the uncertainty on the ^{20}Ne/^{22}Ne ratio.

Table S2: He and Ne data in aerogel samples. Abundances are in units of 10^{-15} mol

Sample	**area mm^2**	**^{4}He**	**+/-**	**^{20}Ne**	**+/-**	**^{20}Ne/ ^{22}Ne/**	**+/-**	**^{21}Ne/ ^{22}Ne**	**+/-**
Instrumental blank (n= 6)		4.9	2.9	0.86	0.20	9.68	0.24	0.0210	0.0130
blank flight aerogel #1	0.42	12.4	7.3	1.17	0.27	9.64	0.36	0.0243	0.0023
c2044,0,41; tile 44, track 7, "Thera 1"	0.26	36.0	2.0	2.27	0.11	10.97	1.12	0.0243	0.0024
Thera 1 corrected for blank		23.6	7.6	1.10	0.29	12.86	3.20	0.0245	0.0029
blank flight aerogel #2	0.06	2.8	1.7	1.03	0.05	9.35	0.11	0.0305	0.0011
c2044,0,41; tile 44, track 7, "Thera 2"	0.30	10.6	0.53	3.61	0.18	10.14	0.12	0.0293	0.0011
Thera 2 corrected for blank		7.8	1.7	2.58	0.19	10.49	0.24	0.0279	0.0017
Air						9.80		0.0292	
Solar						13.8		0.0330	

In a $^{22}Ne/^{20}Ne$ versus $^{4}He/^{20}Ne$ mixing diagram (Fig. S1), data appear significantly different from the atmospheric values and are most consistent with a cometary end-member having a solar Ne isotopic composition (although the data do not allow one to constrain other potential ET end-members) and a $^{4}He/^{20}Ne$ ratio of about 20, the mixing line constructed with this value fitting best the two data points (Fig. S1).

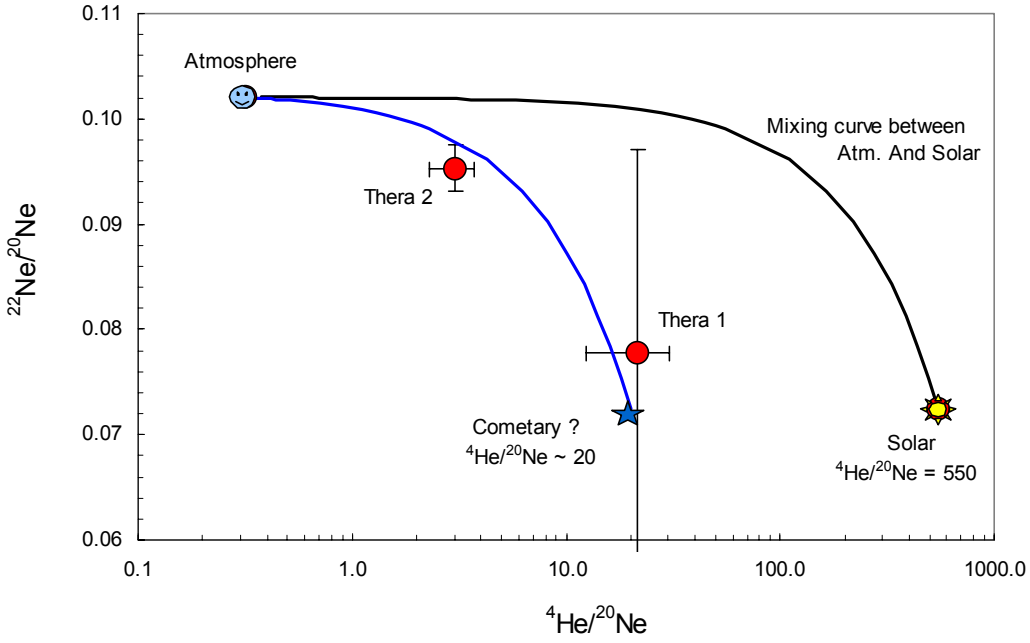

Figure S1: The $^{20}Ne/^{22}Ne$ ratio as a function of the $^{4}He/^{20}Ne$ ratio. The black curve represents mixing between the atmospheric component and the Solar component, and the blue curve is mixing between the atmosphere and a component having a solar $^{20}Ne/^{22}Ne$ ratio and a $^{4}He/^{20}Ne$ ratio of 20 and was adjusted to fit the two data points.

Oxygen isotopic composition of aerogel

The oxygen isotope composition of flight aerogel was determined by laser-assisted fluorination mass spectrometry. Stardust silica aerogel sample b#40, 2393-911 was cut by a razor blade and weighed into 1-2 mg-sized chunks, placed in a small open box (Au-foil), and kept dry overnight in a 60°C oven. The box was introduced into the reaction chamber of a vacuum fluorination line under dry nitrogen gas flow. The reaction chamber was evacuated until a vacuum of better that 1×10^{-6} mbar was achieved. The sample chamber was then continuously pumped for 2 days, during half of which it was externally heated (IR-lamp) to 50°C.

Fluorination of crystalline material requires that the evacuated reaction chamber and samples are pretreated with an aliquot of F_2, usually overnight. This is to ensure that any contamination introduced into the chamber during sample insertion will react with F_2, and then be pumped away. However, due to the high surface area of the silica aerogel, and its extreme reactivity, this step led to partial reaction of the F_2 with the aerogel test samples, liberating oxygen prior to the actual laser-fluorination. Tests showed that the

extended evacuation and heating to 50°C is sufficient to achieve the same low levels of contamination afforded by F_2-pretreatment.

Laser-fluorination was carried out using a 25 W CO_2 laser that heats the sample in an atmosphere of 50 mbar purified F_2. Excess F_2 was removed by reaction of the O_2/F_2 mixture with KBr. The oxygen was then purified by absorption on a 13X molecular sieve at –190°C, followed by elution of the O_2 from the first sieve at –131°C to a second 5A molecular sieve at –190°C. This step removes trace amounts of NF_3 by retention on the first sieve, permitting separation of O_2 and NF_3 and ensuring that the analyte O_2 is free from interferences that compromise the accuracy of $\Delta^{17}O$ measurements (NF^+ is an isobar for $^{33}O_2^+$ on the gas-source mass spectrometer). The oxygen was then admitted directly to a Finnigan DeltaPlus dual inlet isotope ratio mass spectrometer for measurement of the isotope ratios. Each sample gas was analyzed multiple times (n in Table S3), each analysis consisting of 20 cycles of sample-standard comparison.

The oxygen isotope ratios are calibrated against the isotopic composition of air O_2 and San Carlos olivine. For tropospheric oxygen we obtain $\delta^{18}O$ and $\delta^{17}O$ values of 23.51 ± 0.01 ‰ and 11.97 ± 0.03 ‰ respectively (the negative $\Delta^{17}O$ of tropospheric air relative to rocks is well known). A typical analysis of San Carlos olivine in our lab gives $\delta^{18}O$ = 5.32 ± 0.01 ‰ and $\delta^{17}O$ = 2.75 ± 0.04 ‰.

Table S3: oxygen isotopic composition of flight aerogel

	wt.		yield**	$\delta^{17}O'$		$\delta^{18}O'$		$\Delta^{17}O'$		
date	(mg)		(%)	mean	st.dev.	mean	st.dev.	mean	st.dev.	n
12-Aug-06	1.21		86	-0.462	0.033	-0.987	0.026	0.060	0.029	7
16-Aug-06	1.91		72	-0.571	0.017	-1.184	0.020	0.055	0.023	12
			average	-0.516		-1.086		0.057		
			st.dev.	0.077		0.139		0.003		

*=pressure of sample O2-gas in mass spectrometer bellow

**=aerogel yield estimated by assuming a SiO_2 formula unit.

Oxygen isotope analyses

High precision oxygen isotope analyses were made using the Cameca ims 1270 instruments at the Centre de Recherches Pétrographiques et Géochimiques, Nancy, and at the University of California, Los Angeles. The enstatite grain (T69) was embedded in acrylic, ultra-microtomed, extracted from acrylic using acetone, transferred and pressed onto gold foil. Some fragments of acrylic were still present around the grains and the acrylic had been annealed locally by the electron beam used to perform electron microprobe analyses. No additional cleaning was performed on the grain before the introduction of the gold foil in the ion microprobe. The forsterite-rich grain (T22) was extracted from aerogel using a fine needle, and then pressed into clean gold foil. No attempt was made to remove adhering aerogel. The refractory particle "Inti" was potted in acrylic for ultramicrotomy and the remainder of the cut section was cut off and pressed into In and coated with a thin layer of Au for ion probe analysis.

Isotopic measurements were made by sputtering with a 20keV, ~0.1 – 0.2 nA Cs^+ beam. Spot size was about ~8-10 μm for the analyses of T22 and T69 and the first run on

Inti; for the second set of analyses on Inti the beam was better focused to ~5 μm resulting in essentially no overlap with aerogel adhering to the particle, but still incorporating a mixture of mineral phases from the particle. For all analyses, low-energy negative secondary ions were accelerated to 10 keV and analyzed at high resolving power ($m/\Delta m > 6500$) in order to separate all interfering molecular species ($^{16}OH^-$, $^{17}OH^-$, $^{16}OH_2^-$) from atomic oxygen ions and a normal-incidence electron gun was utilized for charge compensation. A Faraday cup (FC) detector was used to measure $^{16}O^-$ current, while the ion beams for the minor isotopes ^{17}O and ^{18}O were measured by pulse counting with electron multipliers (EM). Ion intensities were corrected for background (FC) and deadtime (EM). Instrumental mass fractionation (IMF) and relative detector efficiencies were corrected by comparison to measurements made on terrestrial standards (mantle olivine and pyroxene, as well as hibonite and spinel) interspersed with those of the unknowns. Quoted uncertainties are 2 standard error of the mean and incorporate external reproducibility on standards.

One analysis was made on acrylic fragments which are present in the vicinity of the enstatite grain T69 to evaluate possible contamination from the acrylic during the analysis. The measured $\delta^{17}O$ (-19.5 ± 1.2 ‰) and $\delta^{17}O$ (-33.5 ± 0.5 ‰) are very negative (when corrected with instrumental mass fractionation determined on enstatite) probably reflecting large matrix effects on instrumental mass fractionation (although the oxygen isotope composition of the acrylic is not known). Oxygen emissivity from the acrylic was high (on the order of a factor of 20% to 50% of the signal from silicates) so that its contribution to the total O signal cannot be neglected.

Table S4. Oxygen isotopic compositions of comet 81P/Wild2 grains.

Sample	$\delta^{18}O$ (‰)	$\delta^{17}O$ (‰)	phases analyzed
C2115,1,22,0 (Track 22):			
spot 1	-1.7 ± 1.2	-1.5 ± 1.6	10 μm grain; Mg-rich olivine with
spot 2	2.2 ± 1.2	0.4 ± 1.7	minor pyroxene
spot 3	-6.0 ± 1.1	-2.6 ± 1.7	affected by aerogel contamination
C2027,2,69,1,0 (Track 69):			
run 1, spot 1	-0.3 ± 0.4	-0.8 ± 0.9	low-Ca pyroxene
run 1, spot 2	4.5 ± 0.4	-0.1 ± 0.9	
run 2, spot 1	1.1 ± 0.4	-1.1 ± 1.1	
	-5.2 ± 0.6	-3.8 ± 1.7	acrylic contamination evident
	-6.9 ± 0.5	-4.9 ± 1.2	acrylic contamination evident
	-8.8 ± 0.8	-6.8 ± 1.7	acrylic contamination evident
Acrylic embedding medium			
	-33.5 ± 0.5	-19.5 ± 1.2	
C2054,4,25,1,0 (Track 25, "Inti"):			
run 1, spot 1	-39.5 ± 1.0	-39.4 ± 4.3	10 μm refractory particle
run 1, spot 2	-36.1 ± 2.4	-38.7 ± 3.8	some aerogel contamination possible
run 2, spot 1	-40.9 ± 1.3	-40.5 ± 1.6	mix of melilite, anorthite, and spinel
run 2, spot 2	-41.6 ± 1.3	-42.0 ± 2.5	(see Zolensky et al., this volume)

Six analyses were made on the enstatite grain (T69) at different locations on the grain (Table S4). The positions of the spot were chosen in order to try to maximize the count rate on oxygen, while minimizing overlap of the beam with acrylic. The measured oxygen isotope composition show a range of variations (Fig S2, Table S4) which most likely reflects the mixing under the ion probe beam of various proportions of enstatite and acrylic. The 3 analyses which show minimal mixing effects are plotted in Fig. 4; all analyses are shown in Fig. S2. The two analyses of a forsterite grain (T22) show minimal contamination from adhering aerogel.

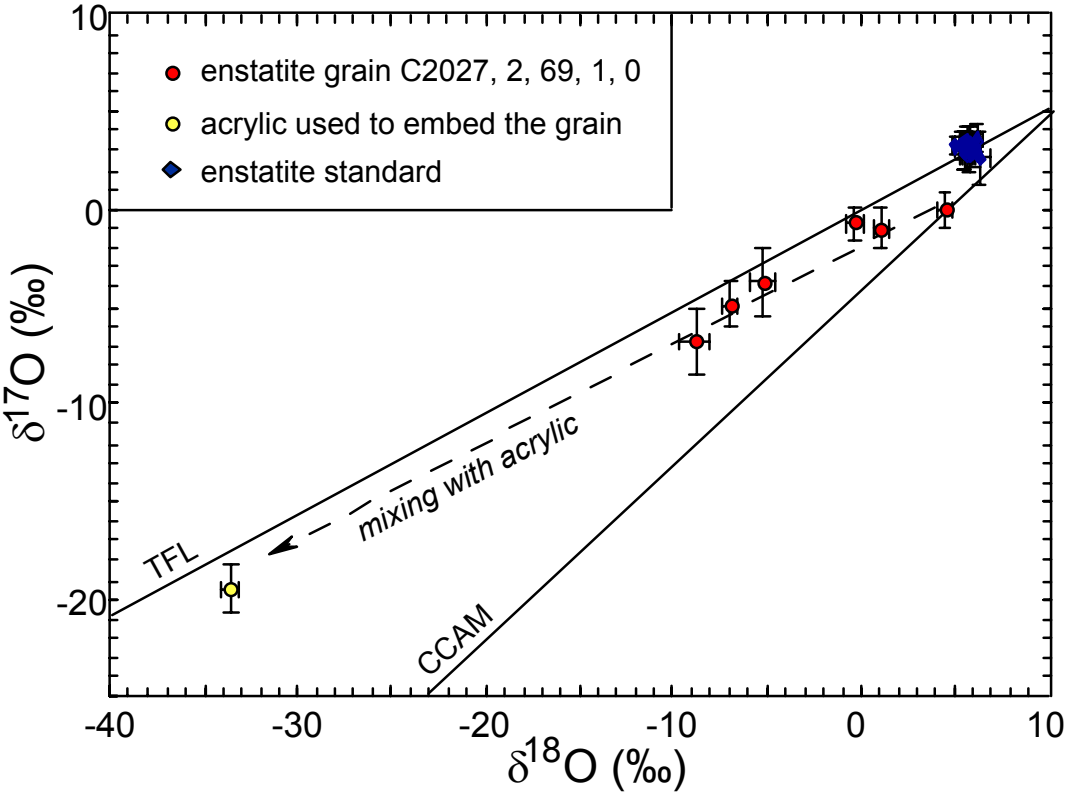

Figure S2. Three oxygen isotopes diagram showing the composition of the six spots made on Stardust enstatite grain C2027, 2, 69,1, 0 (Track 69). The terrestrial fractionation line (TFL) and the carbonaceous chondrites anhydrous minerals line (CCAM) are shown for reference. The range of variation observed is likely due to mixing under the ion probe beam with fragments of acrylic used to embed the grain. The least contaminated spot lies on the CCAM line.

Samples were also analyzed for C, N and O isotope compositions using the Cameca NanoSIMS 50 at Lawrence Livermore National Laboratory. Isotope abundances were determined by quantitative ion imaging using a ~0.6 to 1.2 pA, 16 keV $^{133}Cs^{+}$ primary ion beam focused into a ~100 nm spot and rastered over areas ranging in size from 4 x 4 to 13 x 13 μm^2, depending on the size of the sample and extent of contamination by aerogel or acrylic. An electron food gun was used to provide charge compensation for O-isotope

analyses of some samples. Scan rates were variable, depending on image size and secondary intensity, with dwell times of 1 to 5 ms per pixel. Secondary ion intensities for $^{12}C^-$, $^{13}C^-$, $^{16}O^-$, $^{17}O^-$, $^{18}O^-$, $^{12}C^{14}N^-$, and $^{12}C^{15}N^-$, together with secondary electrons, were collected simultaneously (5 species at a time) in multi-collection mode at a mass resolving power of ~6500, sufficient to separate $^{13}C_2$ from $^{12}C^{14}N$, and $^{12}C^{15}N$ from $^{13}C^{14}N$. Three difference sequences of masses were measured: ^{16}O, ^{17}O, ^{18}O and ^{28}Si for O-isotopes; ^{16}O, ^{17}O, ^{18}O, $^{12}C^{14}N$ and $^{12}C^{15}N$ for O and N isotopes; and ^{12}C, ^{13}C, ^{16}O, $^{12}C^{14}N$ and $^{12}C^{15}N$ for C and N isotopes; secondary electron images were collected with each sequence. The isotope imaging measurements consist of 40 to 100 scans over each region of interest; the scans are subsequently added together to create a single image for each area. The data are processed as quantitative isotope ratio images using custom software. Isotope ratio images are obtained by dividing the images of two species, e.g., ^{12}C and ^{13}C, pixel by pixel, and are corrected for image drift and statistical outliers. Typically, the data are smoothed using a 4 x 4 pixel^2 integration area. The C, N, and O isotope ratios measured in Stardust samples are calibrated to ratios measured in standards: NIST SRM-24 graphite for C, NIST SRM-8558 KNO_3 embedded in SRM-24 graphite and Mahakam Delta 48055 type III kerogen crushed on gold for N, and aerogel for O. The NanoSIMS O-isotope data reported here were renormalized to the ims-1270 data for "Inti" to correct for mass-dependent fractionation. The normalized ratios are reported using delta notation (permil deviation from the appropriate standard). Uncertainties in isotope ratios are reported as 2 standard deviations and include counting statistics errors on individual measurements propagated with the reproducibility of replicate measurements of the standards.

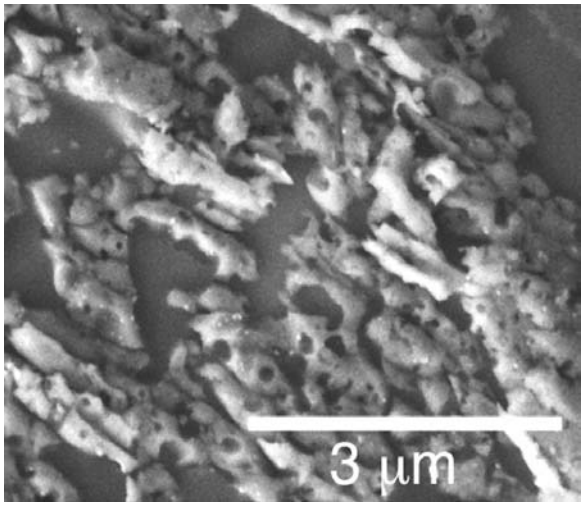

Fig. S3. Secondary electron image of a microtomed slice of particle C2025W showing vesicular glass embedded in epoxy (smooth areas). Numerous, small sulfide inclusions are visible entrained in glass.

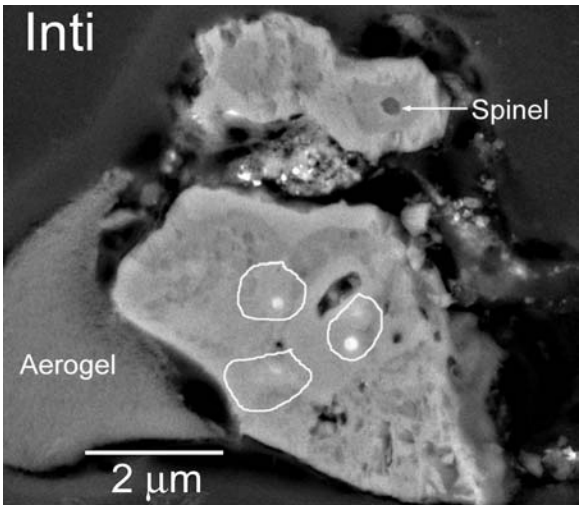

Fig. S4. Secondary electron image of a polished fragment of the refractory inclusion Inti; see Zolensky et al. (this volume) for a discussion of the mineralogy. Areas analyzed for O-isotopes are outlined.

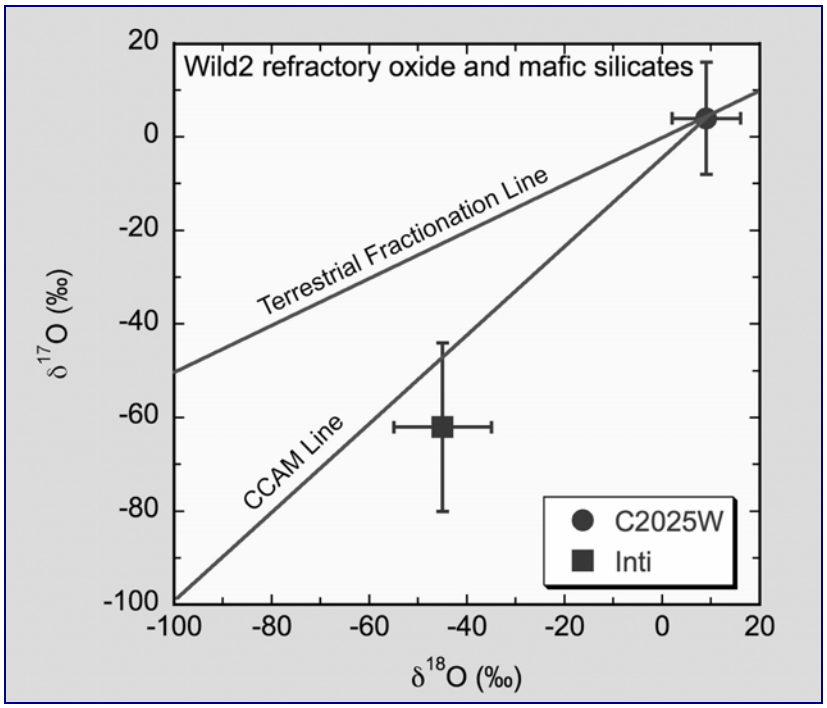

Fig. S5. Oxygen isotope compositions of refractory inclusion "Inti" and Mg-rich vesicular glass, determined by NanoSIMS. Inti is enriched in ^{16}O, similar to refractory inclusions in chondritic meteorites, while the vesicular glass has a composition similar to mafic silicates in carbonaceous chondrites. Uncertainties are 2σ.

O-isotope abundances were measured in 4 microtomed slices (serial sections) of a fine-grained "particle" consisting of Mg-rich vesicular glass containing numerous sulfide inclusions and in two microtomed slices of the "Inti" refractory inclusion (Figs. S3, S4); a polished "thick" section of Inti was subsequently analyzed with the ims-1270 at UCLA. O-isotope ratio images of 4 sections of vesicular glass show no evidence for isotope heterogeneity within a measurement precision of 4-6% at the 200 nm spatial scale. The average composition defined from 7 isotope ratio images reveals a composition consistent with average chondritic material and plots along the terrestrial fractionation (TF) line with $\delta^{17}O = 4\pm12‰$ and $\delta^{18}O = 9\pm7‰$. In contrast, the O-isotope ratio images of "Inti" show clear evidence of ^{16}O enrichment and define a composition plotting along the CCAM line with $\delta^{17}O = -62\pm20‰$ and $\delta^{18}O = -42\pm10‰$ (Fig. 2). The relationship seen here between mafic silicates with $\Delta^{17}O \sim 0‰$ and Ca-Al-rich refractory material with $\Delta^{17}O \sim -40‰$ is strikingly similar to that observed in carbonaceous chondrites.

Nitrogen and carbon isotope analyses

N- and C-isotope abundances were measured in the fine-grained vesicular glass described in the preceding paragraph. The C and N secondary ion signals are both very low, reflecting the low abundance of carbon in the glass. Based on the $^{12}C^-/^{14}N^-$ ratio, we estimate the N abundance as ~900 ppm. This N concentration is 10 to 100 times lower

than that found in D-rich and ^{15}N-rich organic material from chondritic IDPs. Due to the low abundances, differentiating C and N indigenous to Stardust material from terrestrial contamination is challenging. The carbon isotope abundances are indistinguishable from normal terrestrial material. Nitrogen, in contrast, exhibits anomalous isotope abundances both on the scale of the whole particle, $\delta^{15}N = 108 \pm 10$ ‰, and in isolated "hotspots" with sizes of ~200 to 800 nm; $\delta^{15}N$ values for 82 localized regions range from -260‰ to +970‰. ^{15}N-enriched regions are more prevalent and the weighted mean $\delta^{15}N$ of all 82 hotspots is 320±24 ‰. The range of $\delta^{15}N$ values is similar to that observed in chondritic IDPs *(Aléon et al., 2003)*. The ^{15}N excesses appear to be associated with carbonaceous material characterized by C and N concentrations equal to or lower than those found in typical kerogens.